Parvalbumin-Expressing Interneurons Linearly Transform Cortical Responses to Visual Stimuli

Bassam V. Atallah[1,*], **William Bruns**[2], **Matteo Carandini**[3], and **Massimo Scanziani**[2,*]

[1]Computational Neurosciences Graduate Program, University of California San Diego, La Jolla, California, 92093-0634, USA

[2]Howard Hughes Medical Institute and Center for Neural Circuits and Behavior and Neurobiology Section, Division of Biology, University of California San Diego, La Jolla, California, 92093-0634, USA

[3]UCL Institute of Ophthalmology, University College London, London EC1V 9EL, UK

Summary

The response of cortical neurons to a sensory stimulus is shaped by the network in which they are embedded. Here we establish a role of parvalbumin (PV)-expressing cells, a large class of inhibitory neurons that target the soma and perisomatic compartments of pyramidal cells, in controlling cortical responses. By bidirectionally manipulating PV cell activity in visual cortex we show that these neurons strongly modulate layer 2/3 pyramidal cell spiking responses to visual stimuli while only modestly affecting their tuning properties. PV cells' impact on pyramidal cells is captured by a linear transformation, both additive and multiplicative, with a threshold. These results indicate that PV cells are ideally suited to modulate cortical gain and establish a causal relationship between a select neuron type and specific computations performed by the cortex during sensory processing.

Introduction

Inhibition in the cortex is generated by a variety of different types of GABAergic interneurons. Determining how each of these interneuron types transforms sensory responses is central to establishing a mechanistic understanding of cortical processing. To date, however, the specific role played by these distinct types of inhibitory neurons in sensory processing is still unknown.

Attempts to understand the role of cortical inhibition in sensory processing in vivo have been challenged by the discrepancy between the exquisite specificity of inhibitory circuits and the unspecific nature of the pharmacological tools at hand. While the different subcellular compartments of cortical pyramidal (Pyr) cells are inhibited by distinct GABAergic interneurons, the action of GABAergic antagonists used to experimentally affect inhibition (Sillito, 1975; Katzner et al., 2011) is general and diffuse. This discrepancy has prevented the selective perturbation of inhibitory transmission mediated by specific interneuron types or generated onto a specific cellular compartment.

To circumvent this problem we have directly manipulated the activity of a genetically identified type of inhibitory interneuron, the parvalbumin (PV)-expressing cell, using

---

microbial opsins, and examined the resulting effect on the response of Pyr cells to visual stimuli. This approach has allowed us to bidirectionally control the activity of PV cells in vivo during sensory stimulation and determine how this cell type contributes to the fundamental operations performed by layer 2/3 Pyr cells in primary visual cortex (V1).

Among the various interneurons that inhibit Pyr cells, those that express PV represent up to a half of the GABAergic interneurons in the cortex (Celio, 1986; Gonchar and Burkhalter, 1997; Kawaguchi and Kubota, 1997). PV cells are known to inhibit the somatic and perisomatic compartments of Pyr cells (Kawaguchi and Kubota, 1997), appear to respond less selectively to specific sensory stimulus features as compared to Pyr cells (Sohya et al., 2007; Niell and Stryker, 2008; Kerlin et al., 2010; Cardin et al., 2007), and play a role in shaping the timing and dynamic range of cortical activity (Cobb et al., 1995; Sohal et al., 2009; Cardin et al., 2009; Pouille and Scanziani, 2001; Gabernet et al., 2005; Cruikshank et al., 2007; Pouille et al., 2009). Despite this wealth of knowledge, how PV cells contribute to the operations performed by the cortex during sensory stimulation is not known. Here we show that PV cells profoundly modulate the response of layer 2/3 Pyr cells to visual stimuli while having a remarkably small impact on their tuning properties. This modulation of cortical visual responses by PV cells is described by a linear transformation whose effects are visible in firing rate once above spike threshold and is well captured by a conductance-based model of the Pyr cell. These results indicate that PV cells are ideally suited to modulate response gain, an essential component of cortical computations that changes the response of a neuron without impacting its receptive field properties. Gain control has been implicated, for example, in the modulation of visual responses by gaze direction (Brotchie et al., 1995; Salinas and Thier, 2000) as well as by attention (Treue and Martinez-Trujillo, 1999; McAdams and Maunsell, 1999).

Results

To control the activity of PV cells we conditionally expressed the light-sensitive proton pump Archeorhodopsin (Arch-GFP; to suppress activity; Chow et al., 2010) or the light-sensitive cation channel Channelrhodopsin-2 (ChR2-tdTomato; to increase activity; Boyden et al., 2005; Nagel et al., 2003) in V1 using viral injection into *PV-Cre* mice (Hippenmeyer et al., 2005). Targeted electrophysiological recordings were performed in anesthetized mice under the guidance of a two-photon laser-scanning microscope.

Visual Responses of PV Cells Are Distinct from Those of Pyr Cells

We characterized PV cells in the adult *PV-Cre* mouse line immunohistochemically and electrophysiologically (Figure 1; Figure S1, available online). We fluorescently labeled the cells expressing Cre by crossing *PV-Cre* mice with a *tdTomato* reporter line (Madisen et al., 2010). tdTomato was present exclusively in neurons that were also immunopositive for PV, confirming that cells expressing Cre also expressed PV (97% ± 2%; mean ± standard deviation [SD]; n = 400 cells in 4 mice; Figure S1). Targeted loose-patch recordings from fluorescently labeled PV cells in layer 2/3 of the primary visual cortex in vivo (spontaneous rate: 2.1 ± 3.1 spikes/s; n = 79) showed that their spike-waveforms (Figure S1) had faster kinetics than non-PV cells recorded using the same configuration, consistent with these cells being of the fast-spiking type (McCormick et al., 1985; Connors and Kriegstein, 1986; Swadlow, 2003; Andermann et al., 2004; Mitchell et al., 2007). Because the vast majority (~90%) of the non-PV cells in layer 2/3 are Pyr cells (Gonchar and Burkhalter, 1997), from here on we will refer to non-PV cells as Pyr cells.

PV cells gave strong responses to drifting gratings of various contrasts and orientations presented to the contralateral visual field (evoked rate: 12.1 ± 9.6 spikes/s; n = 79; Figure 1D). Consistent with earlier reports, however, these responses were barely modulated by

stimulus orientation (Sohya et al., 2007; Niell and Stryker, 2008; Kerlin et al., 2010; Zariwala et al., 2011; Ma et al., 2010; Bock et al., 2011; Hofer et al., 2011). To estimate the overall selectivity for stimulus orientation we computed the orientation selectivity index (OSI), the ratio of the modulation in response caused by changing orientation to the average response across orientations. OSI was extremely low for PV cells (0.1 ± 0.1; n = 63), significantly lower than in Pyr cells (0.4 ± 0.2; n = 60; $p < 1 \times 10^{-11}$ Wilcoxon rank-sum test; Figure 1). Only 3% of PV cells, as compared to 65% of Pyr cells, had an OSI > 0.25 (Figure 1D). Furthermore PV cells were more broadly tuned than Pyr cells. To estimate the tuning sharpness we calculated the half width at half height (HWHH) of a double Gaussian fit to the tuning curve of each cell; PV cells: 52 ± 24 degrees; n = 63; Pyr cells: 42 ± 23 degrees; n = 60; $p < 0.05$). Finally, the contrast response function of PV cells differed in two clear ways from that of Pyr cells (Figure 1D). First, the maximal firing rate was two times higher for PV cells than for Pyr cells (9.1 ± 5.6 spikes/s; n = 43; versus 4.5 ± 3.0 spikes/s; n = 30). Second, the increase in firing rate of PV cells with increasing contrast, captured by the exponent of the curve fitted to contrast responses, for PV cells was significantly shallower than for Pyr cells (2 ± 2; n = 43; versus 3.0 ± 2.5; n = 30; $p < 0.005$). Thus, in contrast to a previous report (Runyan et al., 2010) the response properties to visual stimuli of PV cells differ markedly from those of Pyr cells.

Bidirection Control of PV Cell Activity

Next, we assessed the impact of optogenetic manipulation on the visual responses of PV cells. We recorded from Arch- or ChR2-expressing layer 2/3 PV cells at least two weeks after viral injection and illuminated the exposed cortex with a fiber-coupled LED (470 nm, Figure 2). Since strong suppression of inhibition can result in runaway activity (Prince, 1978) and strong activation of PV cells can completely silence cortical activity (not shown), we perturbed PV cell firing over a moderate range chosen to fall within the reported firing rates of these neurons in active awake mice (Niell and Stryker, 2010). Control measurements in uninjected animals established that illumination by itself did not affect visual responses (Figure S5).

Photo stimulation of Arch significantly reduced the firing rate of targeted PV cells, both spontaneous (from 3.0 ± 3.5 to 1.9 ± 3.4 spikes/s; n = 31; $p < 0.02$ paired Wilcoxon sign-rank test) and visually evoked (from 9.2 ± 7.3 to 6.6 ± 7.0 spikes/s; n = 31; $p < 0.0001$; Figure S2A). PV cell firing rate decreased at all contrasts tested (Figure 2D) and was well described by a linear fit ($0.6 \times$ control rate $- 0.4$ spikes/s). Thus, PV cell firing rates decreased by approximately the same factor, 0.6, minus an offset, 0.4 spikes/s, regardless of stimulus contrast (Figure 2D).

Photo stimulation of ChR2-expressing PV cells had the diametrically opposite effect, increasing both their spontaneous firing (from 3.0 ± 3.8 to 5.8 ± 6.1 spikes/s; n = 16; $p < 0.01$) and their visually evoked firing (from 13.6 ± 13.2 to 18.0 ± 15.1 spikes/s; n = 16; $p < 0.01$; Figure S2B). As for Arch-mediated suppression of PV cells, the fractional increase in PV cell firing rate with ChR2 was similar for all presented contrasts (linear fit: $1.2 \times$ control rate $+ 2.0$ spikes/s; Figure 2E).

Thus, we could bidirectionally modulate visually evoked activity of PV cells by approximately the same factor, plus a small offset, independently of how strongly these neurons were driven by the visual stimulus.

PV Cells Tightly Control Visual Responses of Pyr Cells

To assess how PV cell activity impacts cortical responses to visual stimuli, we asked how their suppression or activation changes the visual responses of layer 2/3 Pyr cells. We

concentrated on three response attributes: response to contrast, overall selectivity for orientation and direction, and sharpness of tuning.

Optogenetic modulation of PV cell activity strongly affected the response of Pyr cells to visual stimuli. Suppressing PV cell activity by photo stimulating Arch led to an increase in the spike rate of Pyr cells (change in firing rate: 0.8 ± 1.5 spikes/s; $73\% \pm 85\%$; n = 43 cells; $p < 0.005$; Figure S2C). This increase was again well described as a linear transformation ($1.4 \times$ control rate + 0.3 spikes/s) independently of the contrast tested (Figure 2F). Complementarily, activating PV cells by photo stimulating ChR2 resulted in decreased Pyr cell spike rates (change in firing rate: -3.7 ± 2.2 spikes/s; $-38\% \pm 30\%$; n = 19 cells, $p < 0.005$; Figure S2D), again at all contrasts tested ($0.7 \times$ control rate − 0.3 spikes/s; Figure 2G).

These results indicate that PV cells tightly control the response of Pyr cells, and they do so in a manner that is independent of stimulus contrast. Indeed, manipulation of PV cell activity scaled the response of Pyr cells, with little effect on the shape of their contrast responses curves. PV cells, therefore, control the response but not the contrast sensitivity of Pyr cells.

PV Cells Only Modestly Impact Pyr Cell Orientation Tuning

Despite the strong influence of PV cells on the firing rate of Pyr cells, bidirectional modulation of PV cell activity only modestly impacted the tuning of Pyr cells for stimulus orientation. Suppression of PV cells with Arch increased Pyr responses to all stimulus orientations (Figure 3A), and activation of PV cells with ChR2 suppressed Pyr responses to all orientations (Figure 3B). Neither manipulation, however, had much of an effect on the shape of Pyr cell tuning curves (see e.g., normalized tuning curves in Figures 3A and 3B). Indeed, the changes in PV activity had hardly had any impact on the relative responses of Pyr cells to each grating direction (Pearson's correlation = 0.8 ± 0.2; n = 45).

Accordingly, PV cell suppression or activation caused only modest changes in the overall selectivity of Pyr cells. Suppression of PV cells with Arch stimulation caused an increase in Pyr firing rate at all orientations. In relative terms, however, it increased responses less at the preferred orientation than at the orthogonal orientation. This resulted in a small but significant decrease of the OSI by -0.06 ± 0.08 (n = 31 Pyr cells; $p < 0.001$; Figure 3C; 13/31 individual cells showed significant changes in OSI). Activation of PV cells with ChR2 led to the opposite effect: a modest (but significant) increase in the OSI of Pyr cells (mean change in OSI: 0.07 ± 0.07; n = 14 cells; $p < 0.003$; 7/14 individual cells showed significant changes; Figure 3B).

These small changes in overall selectivity depended systematically on the change in Pyr cell firing rate caused by PV cell perturbation. A linear regression of the percentage change in spiking response at the preferred orientation versus OSI revealed a highly significant correlation (r = −0.6; n = 45 cells; $p < 0.0001$; Figure 3C). In other words, the Pyr cells that displayed the greatest increase in response also experienced the largest decrease in OSI. Conversely, the Pyr cells that displayed the greatest decrease in response experienced the largest increase in OSI. This said, the changes in OSI were minor even for the largest increases in Pyr cell firing rates: Pyr cells increased their response 3-fold before undergoing a change in OSI of only 0.1, a tenth of the distance separating an untuned cell from a perfectly tuned cell.

As with orientation selectivity, the direction selectivity of Pyr cells changed only modestly while perturbing PV cell activity. Upon PV cell suppression the direction selectivity index (DSI, see Experimental Procedures) decreased by 0.08 ± 0.16 (over the population of n = 31

cells; $p < 0.01$; 7/31 individual cell had significant changes; Figure 3A). Conversely, PV cell activation increased the DSI by 0.07 ± 0.11 (n = 14 cells; $p < 0.05$; 4/14 individual cell had significant changes; Figure 3B). As with OSI, changes in DSI were small but highly significantly correlated with changes in response (r = −0.5; n = 45 cells; $p < 0.001$; Figure 3C).

Remarkably, neither PV cell suppression nor activation had any systematic impact on tuning sharpness. We have already seen that PV cell modulation had no effect on the shape of the Pyr tuning curves for the two example neurons (see normalized tuning curves in Figures 3A and 3B). This effect was common to the whole sample. While perturbing PV cell activity slightly changed the tuning sharpness in a subset of Pyr cells (PV cell suppression: 9/31 cells; ΔHWHH = 7 ± 11 degrees; PV cell activation: 3/14 cells; ΔHWHH = -4 ± 9 degrees), there was no significant impact on the tuning sharpness across the population of Pyr cells (PV cell suppression: HWHH, mean change: 2.5 ± 14.6 degrees; n = 31 cells; $p = 0.5$; PV cell activation: -3.7 ± 8.2 degrees; n = 14 cells; $p = 0.2$). Regression analysis further confirmed that perturbing PV cells did not systematically impact Pyr cell tuning sharpness perturbation ($p = 0.8$; n = 45 cells).

Taken together, these results demonstrate that while PV cells significantly impact the visually evoked responses of layer 2/3 Pyr cells, modulating spiking by as much as 60% below and 250% above baseline rates (Figure 3C), they do so while only modestly impacting orientation and direction selectivity, with no systematic effects on tuning sharpness.

A Linear Function Describes How PV Cells Control Pyr Cell Visual Responses

What is the nature of the transformation performed by PV cells on Pyr cells? We find that a simple function fully captures the impact of PV cells on the responses of Pyr cells to visual stimuli. We plotted the control responses of Pyr cells to stimuli of each orientation (the black points in Figure 4A) against the responses recorded while activating or suppressing PV cells (the red or green points in Figure 4A). Strikingly, the effect of activating or suppressing PV cells on Pyr cell responses was linear (Figure 4B). Suppressing PV cell spiking with Arch linearly increased the activity of Pyr cells: control responses were multiplied by a constant factor of 1.2 and a constant amount was added (Figure 4B, green). Similarly, activating PV cells with Chr2 linearly decreased Pyr cell activity: control responses were multiplied by a constant factor of 0.7 and a constant amount was subtracted (Figure 4B, red). Because suppression of Pyr cells cannot lead to negative firing rates, the lowest control firing rates were suppressed to approximately zero spikes/s. Thus, a simple threshold-linear function with only two parameters (one where the firing rate is zero up to a threshold for activation and then grows linearly) provides a good fit to the data (Figure 4B, lines).

Importantly, the function fully accounts for the observed selective effects of PV cells on Pyr cell responses, with no free parameters (Figure 4C, green and red curves). The function captures the fact that suppression of PV cell activity with Arch linearly scales responses regardless of stimulus orientation (Figure 4). As a result, there is a decrease in overall selectivity for orientation (ΔOSI = -0.11 ± 0.06) but there is no change in tuning sharpness (ΔHWHH = 0 ± 0.1 degrees). Similarly, the function explains that an increase in PV cell activity with ChR2 linearly scales responses regardless of stimulus orientation, except where the responses are pushed below zero (Figures 4B and 4C, gray). As a result, there is an increase in overall selectivity for orientation (ΔOSI = 0.10 ± 0.06) and direction (ΔDSI = 0.04 ± 0.05), again with no change in tuning sharpness (ΔHWHH = 3 ± 5 degrees). Thus, PV cells perform a remarkably simple linear operation on the response of Pyr cells to visual stimuli in layer 2/3 of mouse primary visual cortex.

Suppressing PV Cells Reduce Synaptic Inhibition in Pyr Cells

By what mechanisms do PV cells transform the Pyr cell responses? The suppression of PV cells could in principle have two immediate effects on neighboring Pyr cells: direct reduction in synaptic inhibition and indirect increase in excitation. This indirect effect results from the fact that cortical Pyr cells within layer 2/3 are recurrently connected; thus, an increase in firing rate of Pyr cells in response to PV cell suppression (as observed above) may lead to an increase in the amount of excitation received by the Pyr cells themselves.

To quantify the net decrease in visually evoked inhibition during Arch-mediated suppression of PV cells we recorded in the whole-cell voltage-clamp configuration from layer 2/3 Pyr cells (targeted with two-photon microscopy) using a Cs-based internal solution. When the membrane potential of Pyr cells was clamped at the reversal potential of glutamate-mediated synaptic excitation (~15mV), photo suppression of PV cells decreased by 10% the postsynaptic inhibitory currents evoked by visual stimuli in Pyr cells ($-9\% \pm 20\%$; n = 13 cells, p < 0.03; Figure 5A). To quantify the impact of PV cell suppression on excitation, Pyr cells were voltage clamped at the reversal potential for $GABA_A$ receptor-mediated inhibition (-80mV). Photo suppression of PV cells led to a small but significant increase in spontaneous excitatory conductance (0.1 ± 0.02 nS; n = 10; p < 0.004), demonstrating that our recordings are indeed sensitive to changes in excitation. However no significant increase was measured in visually evoked excitatory conductance (n = 10; p = 0.5; Figure 5B). Thus, PV cell suppression results in little change in excitation but a net decrease in synaptic inhibition on to Pyr cells.

A Conductance-Based Model Captures How PV Cells Transform Pyr Cell Responses

Can this relatively small decrease in inhibition explain the observed linear transformation of Pyr cell spiking activity? To test this we constructed a simple conductance-based model of Pyr cell spiking activity and studied its dependence on stimulus orientation. To fully capture the linear transformation, not only must the decrease in inhibition result in a robust ~ 40% increase in Pyr cells response, but it must do so while having only slight impact on tuning properties and, in particular, tuning sharpness.

To set up the fundamentals of the model we first considered the orientation tuning under control conditions. To this end, we recorded excitatory and inhibitory conductances in layer 2/3 Pyr cells as a function of orientation. Stimulus-evoked excitatory currents (Figure 5C, red trace) recorded at the reversal potential for $GABA_A$ receptor-mediated inhibition showed clear tuning: they were on average 1.7-fold (n = 4) larger at the preferred orientation than at the nonpreferred orientation. In contrast, inhibitory currents (Figure 5C, blue trace) recorded at the reversal potential of glutamate-mediated synaptic excitation were less tuned, being only 1.2-fold (n = 5) larger at the preferred compared to the nonpreferred orientation (consistent with Liu et al., 2010). The membrane potential tuning was then calculated directly from these two opposing conductances (Figure 5D) and the model cell's intrinsic properties (Figure 5E). The spike generation threshold (dotted line, Figure 5E,F) was constrained such that the orientation selectivity and tuning sharpness of spikes matched experimentally measured Pyr cell spike tuning properties (modeled suprathreshold OSI = 0.7 and HWHH = 24 deg; Figure 5F, black trace).

To test the impact of PV cell suppression on model Pyr cell responses, we decreased the inhibitory conductance by 10%, as experimentally determined. Notably, this reduction in inhibition not only resulted in a substantial increase in the modeled spiking response (~50%) but did so in a manner that was strikingly consistent with the experimentally observed linear transformation–i.e., a small decrease in OSI (ΔOSI = 0.08) and no impact on tuning sharpness (ΔHWHH < 2 degrees; Figure 5F, Inset). The model robustly accounted for the

transformation of Pyr cells over the wide range of Pyr cell orientation selectivity (Figure S3).

Thus, this conductance-based model provides insight into how even slight changes in PV cell-mediated inhibition can lead to robust changes in response of Pyr cells to visual stimuli without having a major impact on their tuning properties.

Discussion

By manipulating the activity of PV cells bidirectionally we have determined that while these neurons minimally affect tuning properties, they have profound impact on the response of cortex to stimuli at all contrasts and orientations. We identified a specific and basic computation contributed by these neurons during cortical visual processing: a linear transformation of Pyr cell responses, both additive and multiplicative. This linear transformation of course operates in the presence of a threshold, as firing rates cannot be reduced below zero. The bidirectional control of PV cells during visual stimulation has also allowed us to demonstrate the consistency of this transformation over a range of PV cell activity levels, from ~20% below to 40% above control levels (Figure 2). While suppressing PV cell activity with Arch revealed their function under control conditions, increasing PV cell activity with ChR2 demonstrates their further potential for linearly transforming visual responses in layer 2/3 of the cortex. Finally we showed, using in vivo whole-cell recordings, that the robust changes caused by PV cell perturbation on visually evoked responses in Pyr cells result from relatively small modulations in synaptic inhibition. A conductance-based model provides a likely explanation for how this small yet systematic change in inhibition can lead not only to the observed change in spiking response but also to the observed linear transformation.

Because of their powerful effect on firing rate, minor effect on direction and orientation selectivity and no systematic effects on tuning sharpness, PV-expressing interneurons appear ideally suited to modulate response gain in layer 2/3 of visual cortex (Figure 4). The results obtained here, therefore, provide a causal basis for the view that the response gain of neurons in visual cortex is under the control of GABAa mediated inhibition, as had been postulated based on pharmacological experiments (Katzner et al., 2011). Moreover, our experiments identify a specific role of PV cells in this control of response gain.

Quantification of PV Cell Perturbation

The changes in firing rate that we caused in PV cells are consistent with the changes in inhibitory conductance that we observed in Pyr cells. We chose to perturb PV cells over a moderate range, increasing or decreasing their activity by 3–4 spikes/s (i.e., ~40%; Figures 2D, 2E, and S2) of the average visual evoked firing rate of ~10 spikes/s (Figure 1D). Given that PV cells are 30%–50% of all inhibitory interneurons (Gonchar and Burkhalter, 1997), and that 90% of PV cells were virally infected (88% ± 6%; n = 5 mice), a simple calculation reveals that the observed change in PV cell firing rate should result in a 13% ± 8% change in inhibition, consistent with the experimentally observed 10% reduction in synaptic inhibitory current (Figure 5A). Moreover, since our perturbation of PV cells was chosen to be moderate, and thus fall within the range of firing rates spanned by these neurons during awake-behaving states in mice (Niell and Stryker, 2010), we believe that PV cells are likely to exhibit a similar level of control over visually evoked responses during naturally occurring behavioral states and visual environments.

While changing the firing rate of the PV cells by 3–4 spikes/s (~40%) resulted in an opposite change in layer 2/3 Pyr cell responses by ~0.5–1 spikes/s (~40%; Figures 2F, 2G, and S2), a small fraction (<10%) of Pyr cells exhibited "paradoxical" effects. That is, upon

photo stimulation of Arch-expressing PV cells these Pyr cells were also suppressed rather than activated, or upon photo stimulation of ChR2-expressing PV cells Pyr cells were activated rather than suppressed (Figures 2F, 2G, and S2). These paradoxical effects in Pyr cells probably occur because a small subset (<10%) of PV cells also exhibited paradoxical effects. That is, upon photo stimulation, a few visually identified Arch-expressing PV cells were activated rather than suppressed or ChR2-expressing PV cells were suppressed rather than activated (Figures 2E and S2A). This may be explained by the fact that PV cells not only contact Pyr cells but also inhibit one another (Galarreta and Hestrin, 2002). Thus, in a fraction of PV cells the changes in synaptic inhibition caused by perturbing PV cell activity may outweigh the direct effects of opsin activation. The potential for paradoxical effects during optogenetic manipulation further highlights the importance of directly quantifying the impact of the perturbation.

Perturbing PV Cells Affects Synaptic Inhibition with Little Change in Excitation

We find that PV cells substantially impact the response of layer 2/3 Pyr cells to visual stimuli. In principle, this action can occur via two mechanisms: the direct reduction in synaptic inhibition and, due to the recurrent nature of the layer 2/3 circuit, the indirect increase in excitation. Whole-cell recordings from Pyr cells upon photo suppression of PV cell activity revealed a systematic, yet relatively small, decrease in synaptic inhibition and negligible changes in excitation. This underscores the exquisite sensitivity of cortical sensory responses to even small changes in synaptic inhibition. The fact that synaptic excitation did not change in a consistent manner, despite clear increases in Pyr cell spiking, implies that recurrent excitatory connections between layer 2/3 Pyr cells contribute little to the overall excitatory input onto these cells during visual stimulation, as suggested by a recent study (Hofer et al., 2011).

PV Cells Linearly Transform Visual Responses of Pyr Cells

The computation performed by PV cells, i.e., how these neurons control the visual responses of layer 2/3 Pyr cells, is quantitatively summarized by a simple linear equation, both additive and multiplicative with a threshold (which accounts for the spiking threshold of neurons). While Pyr cell responses are most significantly transformed by the multiplicative factor, which has no impact on tuning properties, the small additive component of this transformation accounts for the minor changes in overall selectivity (quantified by OSI and DSI) while leaving tuning sharpness unchanged.

The simplicity of this transformation relies in part on the fact that, in mice, PV cells generate inhibition that varies little with orientation (Figure 1; Sohya et al., 2007; Niell and Stryker, 2008; Kerlin et al., 2010; Ma et al., 2010). Accordingly, within each condition (control or Arch or ChR2 stimulation), as long as the stimuli were presented at constant contrast (Figure 4) the activity of PV cells must have been approximately constant, regardless of stimulus orientation. In other species, like cats, where due to the presence of large orientation domains the responses of inhibitory neurons are tuned to orientation (Anderson et al., 2000) (although PV cells are likely to be less turned than other neurons; Cardin et al., 2007; Nowak et al., 2008), more complex models may be necessary to describe their impact on visual responses (Ferster and Miller, 2000; Katzner et al., 2011). In the primate, however, where orientation domains have an anatomically smaller scale (Nauhaus et al., 2008), individual PV cells may sample excitation from several domains and, hence similar to mice, control gain by generating orientation invariant inhibition.

Interestingly, despite the fact that cortical responses as a function of contrast and cortical responses as a function of orientation are independent of each other (Niell and Stryker, 2008; Finn et al., 2007), PV cell perturbation affected both responses linearly and in a

quantitatively similar fashion (i.e., PV cell suppression multiplied both responses by ~1.4 and added a small offset). This further demonstrates that PV cells are ideally suited to globally modulate gain.

Modulation of Pyr Cell Response without Systematic Changes in Tuning Sharpness

How can PV cell perturbation so robustly modulate Pyr cell response without systematically affecting tuning sharpness? Based on the classical "iceberg" model of a cell's membrane potential tuning (Carandini and Ferster, 2000) this seems counterintuitive. The iceberg model illustrates the fact that, due to the spike threshold, the spike output of the neuron is generally more sharply tuned than the underlying membrane potential (where a mountain shaped iceberg is the membrane potential tuning curve and the water level is the spike threshold). According to this model, depolarization of the membrane (e.g., by decreasing inhibition through PV cell suppression) is like lowering the water level around the iceberg and results in a broader spiking response as a function of orientation, i.e., a decrease in tuning sharpness. Importantly, this model implies that some of the iceberg is under the water level, i.e., that some of the membrane potential tuning curve is below threshold for spike generation. This is clearly the case in Pyr cells, like the one illustrated in Figures 1E and 1F, that do not generate any spike to stimuli of the nonpreferred orientation. However, such cells are the exception rather than the rule. The average tuning curve of layer 2/3 Pyr cells (e.g., Figure 1D inset and Figure 4) shows that spiking responses are generated even by the nonpreferred orientations, although at much lower rates as compared to preferred orientations. In other words, thanks in part to fluctuations in membrane potential (Carandini, 2007; Finn et al., 2007) the iceberg is almost completely out of the water: further depolarization will increase the firing rate at all orientations but will not result in a broadening of the tuning curve.

Our conductance-based model (Figure 5E) where the membrane potential tuning curve results from experimentally determined excitatory and inhibitory synaptic currents (Figure 5D) illustrates exactly this fact: the membrane potential tuning curve is above threshold at most orientations (arrow in Figure 5E). This mechanism enables PV cells to produce large increases in layer 2/3 Pyr cell response with little impact on tuning sharpness (furthermore, this mechanisms holds over a wide range of OSIs; Figure S3).

Clearly, stronger PV cell activation will eventually enhance tuning sharpness of Pyr cells, as their membrane potential tuning curve is hyperpolarized below threshold. Indeed in 20%–30% of Pyr cells PV cell perturbation led to small yet significant change in tuning sharpness. Overall, however, our results illustrate that perturbing PV cells such as to modulate the response of layer 2/3 Pyr cells over a wide range (from 60% below to 250% above baseline) had no significant effect on the tuning sharpness of the population average, nor resulted in a significant relationship between changes in individual pyramidal cell response and tuning sharpness (Figure 3C).

To our knowledge this is the first time a specific role in cortical sensory processing has been directly attributed to distinct neuron type. PV cells target the somatic and perisomatic compartments of Pyr cells; however, these cells represent only one class among the several types of inhibitory neurons that populate the cortical network (Callaway, 2002; Kawaguchi and Kubota, 1997). Future comparisons between how PV cells and other types of inhibitory cells, such as those that target distinct subcellular domains of Pyr cells, impact visually evoked responses will be exciting.

Experimental Procedures

All procedures were conducted in accordance with the National Institutes of Health guidelines and with the approval of the Committee on Animal Care at UCSD.

Virus Injection

Adult, *PV-Cre* (Jax: 008069), or *PV-Cre x tdTomato* reporter line (Jax: 007908) pigmented mice were anesthetized with 2% isoflurane. Then < 1 mm^2 area of skull over V1 (2 mm lateral to the midline, 0.2 mm rostral to lambda) was thinned and 0.1–0.4 mm^2 craniotomy performed with a 20 G needle. The virus was delivered using a glass micropipette attached to either a Nanoject II (Drummond) or UMP3 (WPI). Over a 10 min period, 100–250 nL of virus AAV2/9.flex.CBA.Arch-GFP.W.SV40 (Addgene 22222) was injected at a depth of 300–500 µm from the cortical surface. We then sutured the scalp, and administered an analgesic (0.1 mg/kg Buprenex) to help the recovery from anesthesia.

AAV2/1.CAGGS.flex.ChR2.tdTomato.SV40 (Addgene 18917) was injected in P0-P1 pups. Pups were anesthetized using a cold pad (0°C). A beveled glass micropipette (tip diameter 40–60 µm) was then used to puncture the scalp and skull and 60 nL injected in three boluses of 20 nL at both 200 and 400 µm below the surface of the scalp.

In Vivo Physiology

Recordings were made from 2- to 8-month-old mice, at least 2 weeks after virus injection. Animals were injected with 5 mg/kg chlorprothixene and 1.5 g/kg urethane. After reaching a surgical plane of anesthesia (10–20 min), the mice were secured with a stereotaxic bite bar, eye-lash hairs were cut, and a thin, uniform layer of silicone oil (30,000 centistokes) was applied to the cornea to prevent drying. The scalp was then removed and a head plate attached with dental cement. A ~1.5 mm^2 craniotomy was performed over V1 (2 mm lateral to the midline, 0.7 mm rostral of lambda). The craniotomy was covered with a thin < 1 mm layer of 1% agarose; dura was left intact for loose-patch recordings and a durotomy performed for whole-cell recordings. Two-photon imaging was performed with a Sutter MOM, coupled to a Coherent Chameleon Laser at 1000–1020 nm. PV cells were targeted based on their expression of tdTomato or eGFP, while Pyr cells were targeted using the "shadow-patching" method (Kitamura et al., 2008; Komai et al., 2006). Targeted recordings were performed using 3–5 MΩ glass electrodes filled with 50 µM Alexa 488/594 or 25 µM Sulfur rhodamine dye in aCSF for loose-patch (in mM: 142 NaCl, 5 KCl, 10 dextrose, 3.1 CaCl$_2$ 1.3 MgCl$_2$, pH 7.4) and Cs-based internal solution for whole-cell voltage-clamp recordings (in mM: 130 Cs-methylsulfonate, 3 CsCl, 10 HEPES, 1 EGTA, 10 phosphocreatine, 2 Mg-ATP, 7.4 pH). Pyr cells were voltage clamped at the reversal potential for excitation (20mV ± 1mV n = 13 cells) and inhibition (−80mV ± 0mV, n = 10 cells) to record inhibitory and excitatory postsynaptic currents (IPSCs and EPSCs), respectively. Series resistance, assessed using an instantaneous voltage step in voltage-clamp configuration, was 31 ± 17 MΩ (n = 21 cells). Voltages were not corrected for the experimentally determined junction potential (−9.8mV ± 0.2mV; n = 3). At the end of the recordings, the animal was sacrificed by administering 2.5% isoflurane followed by decapitation. For histology and/or immunohistochemistry, the brain was extracted, fixed in 4% PFA, and sliced (30 µm).

Visual Stimulation

Stimuli were created using Matlab with Psychophysics Toolbox and displayed with a gamma-corrected LCD screen (Dell 30 × 40 cm, 75 Hz refresh rate, mean luminance 50 cd/m^2) placed 25 cm from the mouse. The preferred spatial frequency (within the range 0.01 and 0.5 cycles/degree) and stimulus size (while ~75% of neurons preferred full-screen

stimuli, the remainder fired more robustly to a smaller circular stimulus of diameter 7–20 degrees) were determined for each neuron. Orientation and direction selectivity was then determined using sinusoidal gratings of 2–3 s duration presented at the preferred spatial frequency, temporal frequency of 2 Hz, 100% contrast, and drifting at 12 randomly interleaved directions. Each stimulus presentation was called a trial. Contrast-response curves were determined by presenting the same drifting grating at the preferred orientation at eight contrast levels logarithmically spanning the range from 1% to 100% contrast.

Photo Stimulation

Photo stimulation of ChR2 or Arch was performed using a 470 nm fiber-coupled LED (1 mm diameter; 0.5 NA; Doric lenses) position approximately 7 mm from the cranial window. Light intensities in the range of 0.1–1 mW/mm^2. To ensure that under our experimental configuration cortical illumination did not itself (in the absence of ChR2/Arch) impact visual responses, we performed control experiments on *PV-CRE* mice that had not received ChR2/Arch virus injection (Figure S5). There were no differences between the control responses (i.e., in the absence of photo stimulation) of in ChR2 versus Arch injected animals for either Pyr (Figure S5) or PV (data not shown) cells.

In Arch- and ChR2-expressing mice we first recorded from PV cells, quantified PV cell suppression/activation and subsequently recorded visually evoked responses in Pyr cells using the same light intensity of photo stimulation. Photo stimulation with light intensities ~0.1–0.5 mW/mm^2 in animals expressing Arch reliably suppressed PV cells, without generating aberrant responses (Figure S4). The level of suppression that we chose was submaximal: rather than completely preventing PV cells from spiking, we reduced their spike rate by ~3–4 spikes/s (Figures 2D and S2; Supplementary Experimental Procedures). Similarly, in animals expressing ChR2 we found that light intensities of ~0.05–0.2 mW/mm^2 would moderately activate PV cells without entirely silencing Pyr responses. So in mice where we did not record from PV cells we used this range of light intensity, i.e., light intensity was set to 0.05–0.1 mW/mm^2, and increased until change in the activity Pyr cells was observed. The population response of the visual cortex to visual stimuli was monitored using local field potential recordings during this process. Light intensities never exceeded 1 mW/mm^2.

When recording from PV cells while photo stimulating Arch or ChR2 (Figure 2) cortical illumination started before the visual stimulus (to monitor the effect on spontaneous activity) and ended before the end of the visual stimulus (to determine the kinetics of recovery to visually evoked firing rates).

Data Analysis

Spontaneous spike rate was calculated as the average firing rate during a 0.5 s period before the presentation of the stimulus. The visual response to a given stimulus was the average rate over the stimulus duration or over the period when both cortical illumination and visual stimulus occurred (1–2 s). Orientation selectivity index (OSI) was calculated as 1 – circular variance (Ringach et al., 1997). Responses to the 12 grating directions were fit with orientation tuning curves i.e., a sum-of-Gaussians (Figures 1, 3, and 4). The Gaussians are forced to peak 180 degrees apart, and to have the same tuning sharpness (σ) but can have unequal height (A_{pref} and A_{null}, to account for direction selectivity), and a constant baseline B. The tuning sharpness was measured as $\sigma (2 \ln(2))^{1/2}$, i.e., the half-width at half height (HWHH). Direction selectivity index (DSI) was calculated as $(R_{pref} - R_{null}) / (R_{pref} + R_{null})$, where R_{pref} is the response at the preferred direction and R_{null} is the response 180 degrees away from the preferred direction. Contrast-response curves were fit with the hyperbolic ratio equation (Albrecht and Hamilton, 1982): $R(C) = R_{max} c^n / (C_{50}^n + c^n) + R_{offset}$, where

c is contrast, C_{50} is the semisaturation contrast, and n is a fitting exponent that describes the shape of the curve, R_{max} determines the gain, and R_{offset} is the baseline response.

To obtain the threshold-linear fit, we first computed a summary of Pyr cell responses in layer 2/3. The tuning curves of all cells were aligned to the same preferred orientation, a nominal value of 0 degrees and the maximal response was scaled to a nominal value of 100% (Figure 4A). We then plotted the median Pyr cell response measured during the suppression or activation of PV cells against the median response measured in the control condition (Figure 4B). The bootstrapped distribution of median responses was used to calculate errors bars in OSI, DSI, and HWHH. Please see Supplemental Experimental Procedures for more details.

Conductance-Based Model

The membrane potential tuning, or net depolarization, as a function of orientation, θ, was modeled as:

$$\Delta V(\theta) = \frac{g_L R_L + g_E(\theta) R_E + g_l(\theta) R_l}{g_L + g_E(\theta) + g_l(\theta)} - V_r$$
$$g_x = g_{min} + (g_{min} - g_{max}) \, e^{\frac{-\theta^2}{2\sigma^2}}.$$

Where x is either E (excitation) or I (inhibition); σ is the tuning sharpness; g_{max} and g_{min} are the conductances at preferred and nonpreferred orientation (see Table 1). R is the reversal potential of the respective conductance. V_r ($-50mV$) is the cell's resting potential.

The firing rate was computed as $[\Delta V(\theta) - V_{thres}]^n_+$, where V_{thres}, the spike threshold, was 4mV (relative to rest) and exponent n was 3 (Priebe et al., 2004). The subscript "+" indicates rectification, i.e., that values below zero were set to zero.

The tuning properties of excitatory and inhibitory synaptic conductances (i.e., σ, g_{min}, g_{max}) in layer 2/3 Pyr cells were determined using whole-cell recordings voltage-clamp configuration where cells were held at the reversal potential for inhibition and excitation, respectively. The average visually evoked conductance was then determined for each of the six orientation of drifting gratings presented (Figure 5C). The result was fit with a Gaussian, g_x.

Statistical significance was determined using the Wilcoxon sign rank, and rank sum tests where appropriate.

Supplementary Material

Refer to Web version on PubMed Central for supplementary material.

Acknowledgments

References

Albrecht DG, Hamilton DB. Striate cortex of monkey and cat: contrast response function. J Neurophysiol. 1982; 48:217–237. [PubMed: 7119846]

Andermann ML, Ritt J, Neimark MA, Moore CI. Neural correlates of vibrissa resonance; band-pass and somatotopic representation of high-frequency stimuli. Neuron. 2004; 42:451–463. [PubMed: 15134641]

Anderson JS, Carandini M, Ferster D. Orientation tuning of input conductance, excitation, and inhibition in cat primary visual cortex. J Neurophysiol. 2000; 84:909–926. [PubMed: 10938316]

Bock DD, Lee WCA, Kerlin AM, Andermann ML, Hood G, Wetzel AW, Yurgenson S, Soucy ER, Kim HS, Reid RC. Network anatomy and in vivo physiology of visual cortical neurons. Nature. 2011; 471:177–182. [PubMed: 21390124]

Boyden ES, Zhang F, Bamberg E, Nagel G, Deisseroth K. Millisecond-timescale, genetically targeted optical control of neural activity. Nat Neurosci. 2005; 8:1263–1268. [PubMed: 16116447]

Brotchie PR, Andersen RA, Snyder LH, Goodman SJ. Head position signals used by parietal neurons to encode locations of visual stimuli. Nature. 1995; 375:232–235. [PubMed: 7746323]

Callaway EM. Cell type specificity of local cortical connections. J Neurocytol. 2002; 31:231–237. [PubMed: 12815242]

Carandini M. Melting the iceberg: contrast invariance in visual cortex. Neuron. 2007; 54:11–13. [PubMed: 17408573]

Carandini M, Ferster D. Membrane potential and firing rate in cat primary visual cortex. J Neurosci. 2000; 20:470–484. [PubMed: 10627623]

Cardin JA, Palmer LA, Contreras D. Stimulus feature selectivity in excitatory and inhibitory neurons in primary visual cortex. J Neurosci. 2007; 27:10333–10344. [PubMed: 17898205]

Cardin JA, Carlén M, Meletis K, Knoblich U, Zhang F, Deisseroth K, Tsai LH, Moore CI. Driving fast-spiking cells induces gamma rhythm and controls sensory responses. Nature. 2009; 459:663–667. [PubMed: 19396156]

Celio MR. Parvalbumin in most gamma-aminobutyric acid-containing neurons of the rat cerebral cortex. Science. 1986; 231:995–997. [PubMed: 3945815]

Chow BY, Han X, Dobry AS, Qian X, Chuong AS, Li M, Henninger MA, Belfort GM, Lin Y, Monahan PE, Boyden ES. High-performance genetically targetable optical neural silencing by light-driven proton pumps. Nature. 2010; 463:98–102. [PubMed: 20054397]

Cobb SR, Buhl EH, Halasy K, Paulsen O, Somogyi P. Synchronization of neuronal activity in hippocampus by individual GABAergic interneurons. Nature. 1995; 378:75–78. [PubMed: 7477292]

Connors BW, Kriegstein AR. Cellular physiology of the turtle visual cortex: distinctive properties of pyramidal and stellate neurons. J Neurosci. 1986; 6:164–177. [PubMed: 3944618]

Cruikshank SJ, Lewis TJ, Connors BW. Synaptic basis for intense thalamocortical activation of feedforward inhibitory cells in neocortex. Nat Neurosci. 2007; 10:462–468. [PubMed: 17334362]

Ferster D, Miller KD. Neural mechanisms of orientation selectivity in the visual cortex. Annu Rev Neurosci. 2000; 23:441–471. [PubMed: 10845071]

Finn IM, Priebe NJ, Ferster D. The emergence of contrast-invariant orientation tuning in simple cells of cat visual cortex. Neuron. 2007; 54:137–152. [PubMed: 17408583]

Gabernet L, Jadhav SP, Feldman DE, Carandini M, Scanziani M. Somatosensory integration controlled by dynamic thalamocortical feed-forward inhibition. Neuron. 2005; 48:315–327. [PubMed: 16242411]

Galarreta M, Hestrin S. Electrical and chemical synapses among parvalbumin fast-spiking GABAergic interneurons in adult mouse neocortex. Proc Natl Acad Sci USA. 2002; 99:12438–12443. [PubMed: 12213962]

Gonchar Y, Burkhalter A. Three distinct families of GABAergic neurons in rat visual cortex. Cereb Cortex. 1997; 7:347–358. [PubMed: 9177765]

Hippenmeyer S, Vrieseling E, Sigrist M, Portmann T, Laengle C, Ladle DR, Arber S. A developmental switch in the response of DRG neurons to ETS transcription factor signaling. PLoS Biol. 2005; 3:e159. [PubMed: 15836427]

Hofer SB, Ko H, Pichler B, Vogelstein J, Ros H, Zeng H, Lein E, Lesica NA, Mrsic-Flogel TD. Differential connectivity and response dynamics of excitatory and inhibitory neurons in visual cortex. Nat Neurosci. 2011; 14:1045–1052. [PubMed: 21765421]

Katzner S, Busse L, Carandini M. GABAA inhibition controls response gain in visual cortex. J Neurosci. 2011; 31:5931–5941. [PubMed: 21508218]

Kawaguchi Y, Kubota Y. GABAergic cell subtypes and their synaptic connections in rat frontal cortex. Cereb Cortex. 1997; 7:476–486. [PubMed: 9276173]

Kerlin AM, Andermann ML, Berezovskii VK, Reid RC. Broadly tuned response properties of diverse inhibitory neuron subtypes in mouse visual cortex. Neuron. 2010; 67:858–871. [PubMed: 20826316]

Kitamura K, Judkewitz B, Kano M, Denk W, Häusser M. Targeted patch-clamp recordings and single-cell electroporation of unlabeled neurons in vivo. Nat Methods. 2008; 5:61–67. [PubMed: 18157136]

Komai S, Denk W, Osten P, Brecht M, Margrie TW. Two-photon targeted patching (TPTP) in vivo. Nat Protoc. 2006; 1:647–652. [PubMed: 17406293]

Liu BH, Li P, Sun YJ, Li YT, Zhang LI, Tao HW. Intervening inhibition underlies simple-cell receptive field structure in visual cortex. Nat Neurosci. 2010; 13:89–96. [PubMed: 19946318]

Ma WP, Liu BH, Li YT, Huang ZJ, Zhang LI, Tao HW. Visual representations by cortical somatostatin inhibitory neurons–selective but with weak and delayed responses. J Neurosci. 2010; 30:14371–14379. [PubMed: 20980594]

Madisen L, Zwingman TA, Sunkin SM, Oh SW, Zariwala HA, Gu H, Ng LL, Palmiter RD, Hawrylycz MJ, Jones AR, et al. A robust and high-throughput Cre reporting and characterization system for the whole mouse brain. Nat Neurosci. 2010; 13:133–140. [PubMed: 20023653]

McAdams CJ, Maunsell JH. Effects of attention on orientation-tuning functions of single neurons in macaque cortical area V4. J Neurosci. 1999; 19:431–441. [PubMed: 9870971]

McCormick DA, Connors BW, Lighthall JW, Prince DA. Comparative electrophysiology of pyramidal and sparsely spiny stellate neurons of the neocortex. J Neurophysiol. 1985; 54:782–806. [PubMed: 2999347]

Mitchell JF, Sundberg KA, Reynolds JH. Differential attention-dependent response modulation across cell classes in macaque visual area V4. Neuron. 2007; 55:131–141. [PubMed: 17610822]

Nagel G, Szellas T, Huhn W, Kateriya S, Adeishvili N, Berthold P, Ollig D, Hegemann P, Bamberg E. Channelrhodopsin-2, a directly light-gated cation-selective membrane channel. Proc Natl Acad Sci USA. 2003; 100:13940–13945. [PubMed: 14615590]

Nauhaus I, Benucci A, Carandini M, Ringach DL. Neuronal selectivity and local map structure in visual cortex. Neuron. 2008; 57:673–679. [PubMed: 18341988]

Niell CM, Stryker MP. Highly selective receptive fields in mouse visual cortex. J Neurosci. 2008; 28:7520–7536. [PubMed: 18650330]

Niell CM, Stryker MP. Modulation of visual responses by behavioral state in mouse visual cortex. Neuron. 2010; 65:472–479. [PubMed: 20188652]

Nowak LG, Sanchez-Vives MV, McCormick DA. Lack of orientation and direction selectivity in a subgroup of fast-spiking inhibitory interneurons: cellular and synaptic mechanisms and comparison with other electrophysiological cell types. Cereb Cortex. 2008; 18:1058–1078. [PubMed: 17720684]

Pouille F, Scanziani M. Enforcement of temporal fidelity in pyramidal cells by somatic feed-forward inhibition. Science. 2001; 293:1159–1163. [PubMed: 11498596]

Pouille F, Marin-Burgin A, Adesnik H, Atallah BV, Scanziani M. Input normalization by global feedforward inhibition expands cortical dynamic range. Nat Neurosci. 2009; 12:1577–1585. [PubMed: 19881502]

Priebe NJ, Mechler F, Carandini M, Ferster D. The contribution of spike threshold to the dichotomy of cortical simple and complex cells. Nat Neurosci. 2004; 7:1113–1122. [PubMed: 15338009]

Prince DA. Neurophysiology of epilepsy. Annu Rev Neurosci. 1978; 1:395–415. [PubMed: 386906]

Ringach DL, Hawken MJ, Shapley R. Dynamics of orientation tuning in macaque primary visual cortex. Nature. 1997; 387:281–284. [PubMed: 9153392]

Runyan CA, Schummers J, Van Wart A, Kuhlman SJ, Wilson NR, Huang ZJ, Sur M. Response features of parvalbumin-expressing interneurons suggest precise roles for subtypes of inhibition in visual cortex. Neuron. 2010; 67:847–857. [PubMed: 20826315]

Salinas E, Thier P. Gain modulation: a major computational principle of the central nervous system. Neuron. 2000; 27:15–21. [PubMed: 10939327]

Sillito AM. The contribution of inhibitory mechanisms to the receptive field properties of neurones in the striate cortex of the cat. J Physiol. 1975; 250:305–329. [PubMed: 1177144]

Sohal VS, Zhang F, Yizhar O, Deisseroth K. Parvalbumin neurons and gamma rhythms enhance cortical circuit performance. Nature. 2009; 459:698–702. [PubMed: 19396159]

Sohya K, Kameyama K, Yanagawa Y, Obata K, Tsumoto T. GABAergic neurons are less selective to stimulus orientation than excitatory neurons in layer II/III of visual cortex, as revealed by in vivo functional Ca2+ imaging in transgenic mice. J Neurosci. 2007; 27:2145–2149. [PubMed: 17314309]

Swadlow HA. Fast-spike interneurons and feedforward inhibition in awake sensory neocortex. Cereb Cortex. 2003; 13:25–32. [PubMed: 12466212]

Treue S, Martinez-Trujillo JC. Feature-based attention influences motion processing gain in macaque visual cortex. Nature. 1999; 399:575–579. [PubMed: 10376597]

Zariwala HA, Madisen L, Ahrens KF, Bernard A, Lein ES, Jones AR, Zeng H. Visual tuning properties of genetically identified layer 2/3 neuronal types in the primary visual cortex of cre-transgenic mice. Front Syst Neurosci. 2011; 4:162. [PubMed: 21283555]
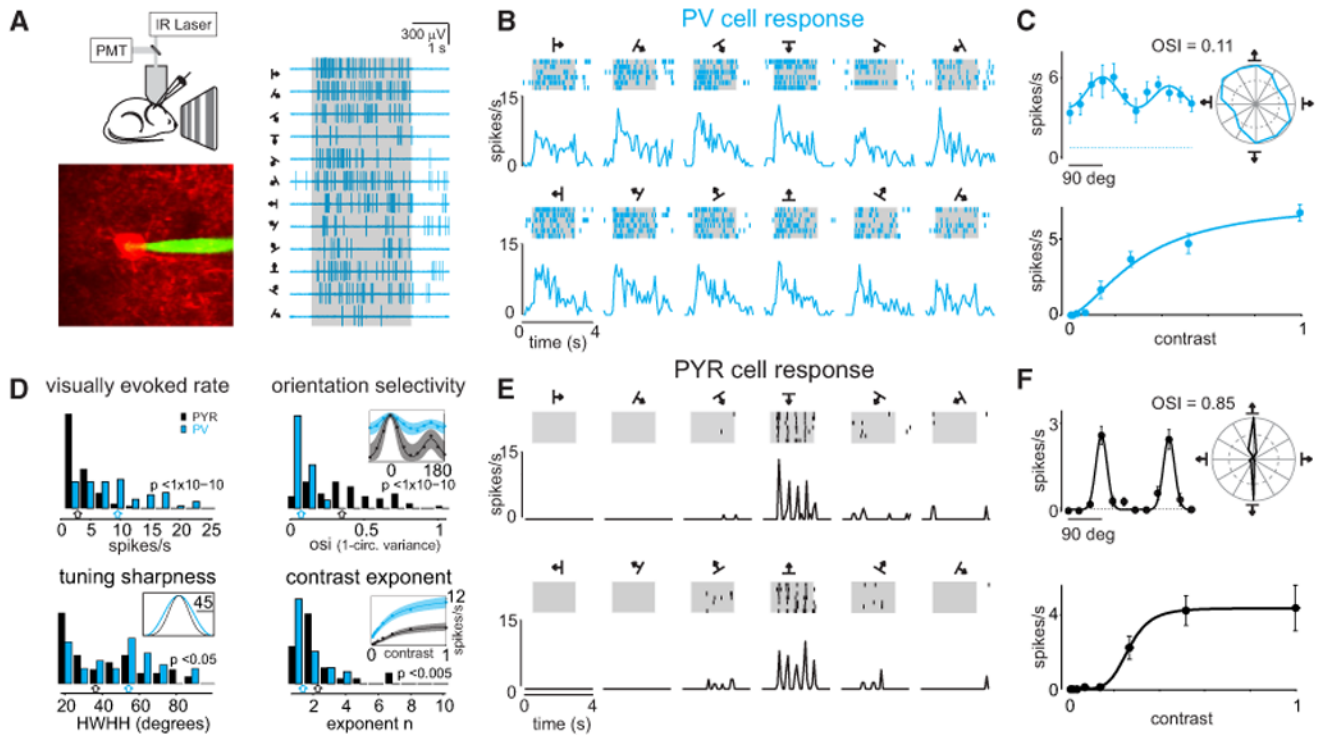
Figure 1. Distinct Visual Response Properties of PV Cells versus Pyr Cells

(A) Left: configuration for two-photon targeted loose-patch recordings in mouse V1; PV cell expressing tdTomato targeted for recording with green electrode. Right: spiking response of the same PV cell to each of 12 directions of a drifting sinusoidal grating (2 s duration, shaded gray box).

(B) Raster plots and peristimulus time-histograms (PSTHs) illustrate the cell's spiking response to repeated grating presentations. Same cell as in (A).

(C) Top: tuning curve, i.e., the average spike-rate during the stimulus presentation of the 12 grating directions, illustrated both on Cartesian and on polar axes (same cell as A). The tuning curve plotted on Cartesian axes is fitted with a double Gaussian. The cell's spontaneous firing rate is illustrated by the dotted line. The cell's poor modulation as a function of orientation is reflected in a low orientation selectivity index (OSI).
Bottom: spiking response of a different PV cell as a function of contrast, fit with a hyperbolic ratio function (line). Error bars are the standard error of the mean (SEM).

(D) Top left: histogram of visually evoked spike rates (PV: n = 79; Pyr: n = 80). Top right: histogram of OSI (PV: n = 63; Pyr: n = 60). Inset: median PV and Pyr cell tuning curves normalized to the peak and fit with double Gaussian (shaded areas illustrated the 2nd and 4th quartile). Note that Pyr cells have a far greater OSI than PV cells. Bottom left: histogram of tuning sharpness, measured as the half-width at half-height (HWHH) of the double Gaussian fit (PV: n = 63; Pyr: n = 60). Inset: median PV and Pyr cell HWHH.
Bottom right: histogram of contrast exponent, n, of hyperbolic ratio fit to contrast response, (PV: n = 43; Pyr: n = 30). Inset: mean PV and Pyr cell contrast response and fit (shaded area is the SEM).

(E) Raster plots and PSTH illustrate the spiking response of a Pyr cell to 12 directions of oriented grating stimuli.

(F) Top: tuning curve of the cell in (E). Note the cell's high OSI as compared to the PV cell in (C). The cell's spontaneous firing rate is illustrated by the dotted line. Bottom: spiking

response of a different Pyr cell as a function of contrast, fit with the hyperbolic ratio function (line). Error bars are the SEM.
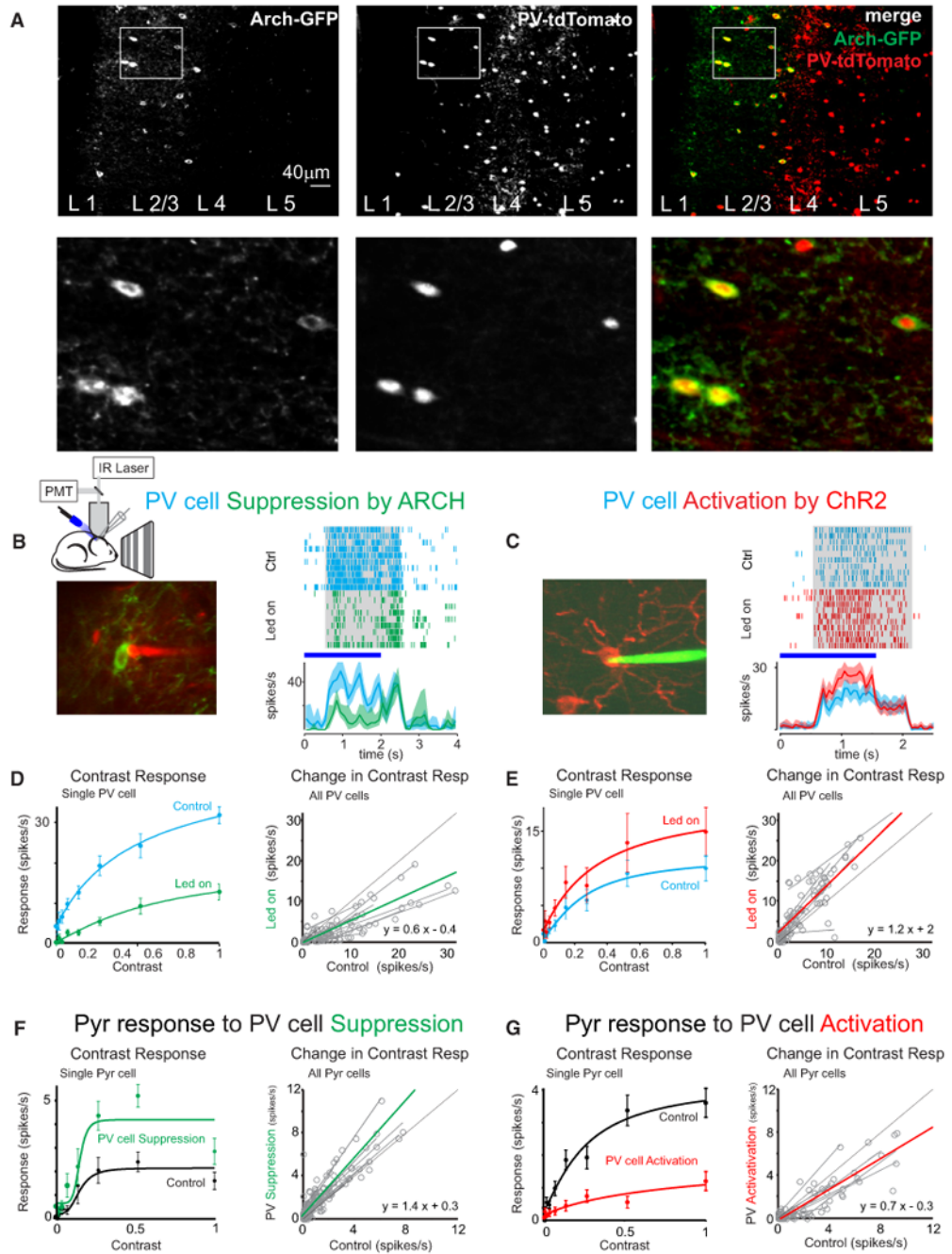
Figure 2. Bidirectional Modulation of PV Cell Activity Demonstrates Their Tight Control of Pyr Cell Contrast Response

(A) Top: coronal section of V1 from a *PV-Cre × tdTomato* reporter mouse injected with Cre depend Arch-GFP AAV-vector. In red: the naive expression of tdTomato; in green: Arch-GFP expressing cells (anti-GFP immunostaining). Bottom: image detail. Note that Arch-GFP expression only occurs in tdTomato expressing, and hence PV expressing, cells.
(B) Left: PV cell expressing Arch-GFP targeted for loose-patch recording with red electrode. Right: raster plot and PSTH of spiking response to grating during interleaved trials: either control (cyan, no led) or during PV cell suppression by Arch photo stimulation (green, LED on). Gray area on the raster plot illustrates the duration of the visual stimulus;

shaded area on the PSTH is the bootstrapped 95% confidence interval (cyan and green). LED illumination is illustrated with horizontal blue bar. Note that the time course of PV cell suppression tightly matches the time course of LED illumination.

(C) Left: PV cell expressing Chr2-tdTomato targeted for loose-patch recording with green electrode. Right: raster plot and PSTH of spiking response to grating during interleaved trials: either control (cyan, no LED) or during PV cell activation with ChR2 photo stimulation (red, LED on). Shaded area and horizontal bar as in (B). Note that the time course of PV cell inactivation tightly matches the time course of led illumination.

(D) Left: example of contrast response of a single PV cell in control (cyan) and during suppression by Arch photo stimulation (green). Error bars are the SEM.

Right, gray: visually evoked spike rate of PV cells under control conditions versus during Arch photo stimulation (circles; 8 different contrasts for each cell; n = 14 cells) Lines: linear fits to each cell; green line: average linear fit; dotted line at unity.

(E) Left: example of contrast response of a single PV cell in control (cyan) and during activation with ChR2 (red). Error bars are the SEM.

Right, gray: visually evoked spike rate of PV cells under control conditions versus during ChR2 photo stimulation (circles; 8 different contrasts for each cell; n = 11 cells). Lines: linear fits to each cell; red line: average linear fit; dotted line at unity.

(F) Left: contrast response of a single Pyr cell in control (black) and during suppression of PV cells (green). Error bars are the SEM.

Right, gray: visually evoked spike rate of Pyr cells under control conditions versus during PV cell suppression (circles; 8 different contrasts for each cell; n = 17 cells). Lines: linear fits to each cell; green line: average linear fit; dotted line at unity.

(G) Left: example of contrast response of a single Pyr cell in control (black) and during activation of PV cells (red). Error bars are the SEM.

Right, gray: visually evoked spike rate of Pyr cells under control conditions versus during PV cell activation (circles; 8 different contrasts for each cell; n = 10 cells). Lines: linear fits to each cell; red line: average linear fit; dotted line at unity.
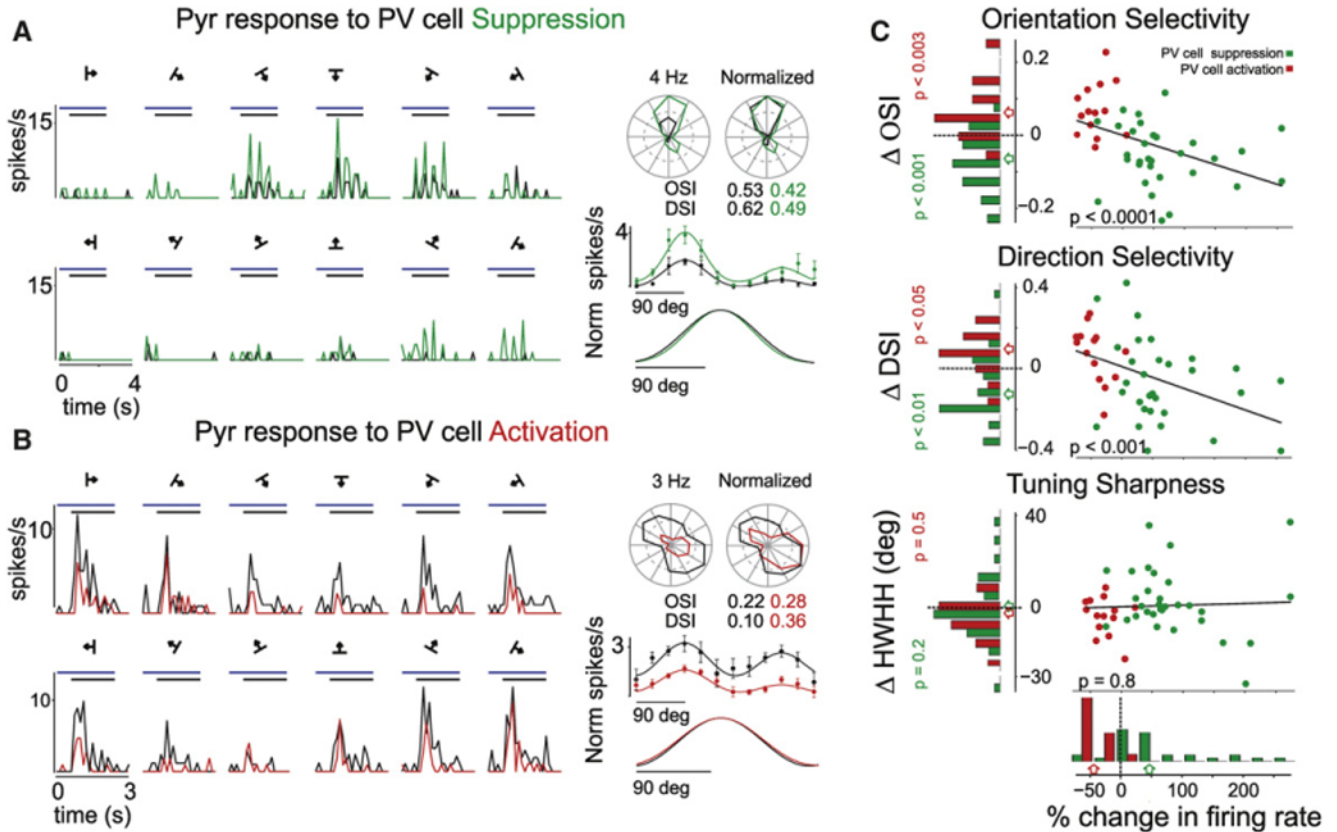
Figure 3. Slight Modulation of Pyr Cell Tuning Properties by PV Cells

(A) Left: PSTH of Pyr cell response to drifting gratings during control (black) or Arch-mediated suppression of PV cells (green). Horizontal bars: black, stimulus presentation; blue, LED illumination. Right: the tuning of the cell is illustrated on polar (top) and Cartesian (middle) axes (black: control; green: PV cell suppression). The tuning curves plotted on Cartesian axes are fitted with a double Gaussian. Note the slight reduction in both orientation and direction selectivity indexes. Bottom: the Gaussian fits under control (black) and PV cell suppression (green) are normalized to the peak and superimposed for comparison. Error bars are the SEM. Note that the tuning sharpness during PV cell suppression remains essentially unaffected.

(B) Left: PSTH of Pyr cell response to drifting gratings during control (black) or ChR2-mediated activation of PV cells (red). Horizontal bars: black, stimulus presentation; blue, LED illumination. Right: the tuning of the cell is illustrated on polar (top) and Cartesian (middle) axes (black: control; red: PV cell activation). The tuning curves plotted on Cartesian axes are fitted with a double Gaussian. Note the increase in both orientation and direction selectivity indexes. Bottom: the Gaussian fits under control (black) and PV cell activation (red) are normalized to the peak and superimposed for comparison. Error bars are the SEM. Note that the tuning sharpness during PV cell activation remains essentially unaffected.

(C) Linear regression (line) of percentage change in Pyr cells firing rate at their preferred orientation versus the change in their tuning properties during PV cell photo suppression (green dots; n = 31) or PV cell photo activation (red dots; n = 14). p values (black) indicate the significance of correlation between in change firing rate and tuning property. Left: distributions of respective tuning properties (negative values indicate decrease in tuning

property; p value indicates confidence that there is a significant difference; green: Arch versus control; red: ChR2 versus control). Bottom: distribution of change in firing rate. Arrows point to population medians.
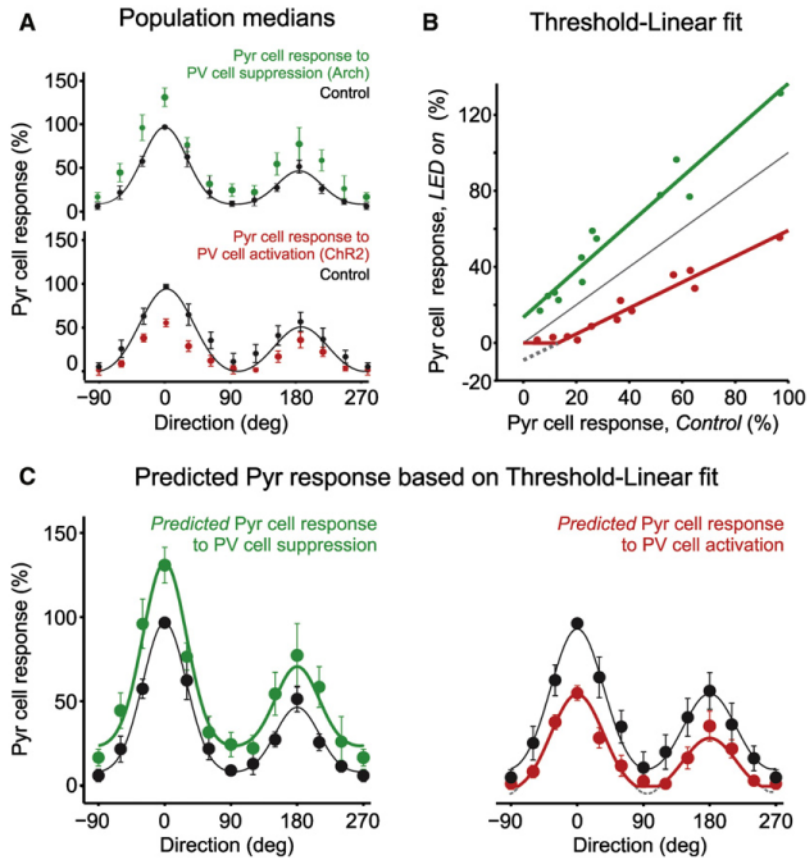
Figure 4. A Linear Function with a Threshold Describes How PV Cells Transform Pyr Cell Responses

(A) Median response of Pyr cell population to 12 directions under control conditions (black circles) and upon PV cell photo suppression (green circles; n = 31) or PV cell photo activation (red circles; n = 14). Error bars are bootstrapped 95% confidence intervals. Black solid lines: double Gaussian fits to median control response.

(B) Median response of Pyr cell population to 12 directions during PV cell photo suppression (green circles) or PV cell photo activation (red circles) plotted against control conditions (same data as A). Solid lines: threshold-linear function fit to data (green: slope of 1.2 and offset of 11%; red: slope 0.7 and offset of –13%). Gray dashed line extends the red linear fit to negative Pyr cell firing rates (i.e., the linear function without applying the threshold). Gray solid line is at unity.

(C) Same data as (A), with the addition of the quantitative prediction of Pyr cell tuning curves (green and red lines) based on the threshold-linear functions in (B).

Note the threshold-linear functions illustrates that activation/suppression of PV cells linearly scales Pyr cell responses regardless of stimulus orientation except where the responses are pushed below zero (gray lines). As a result, there is no change in HWHH and a small change in orientation and direction selectivity.
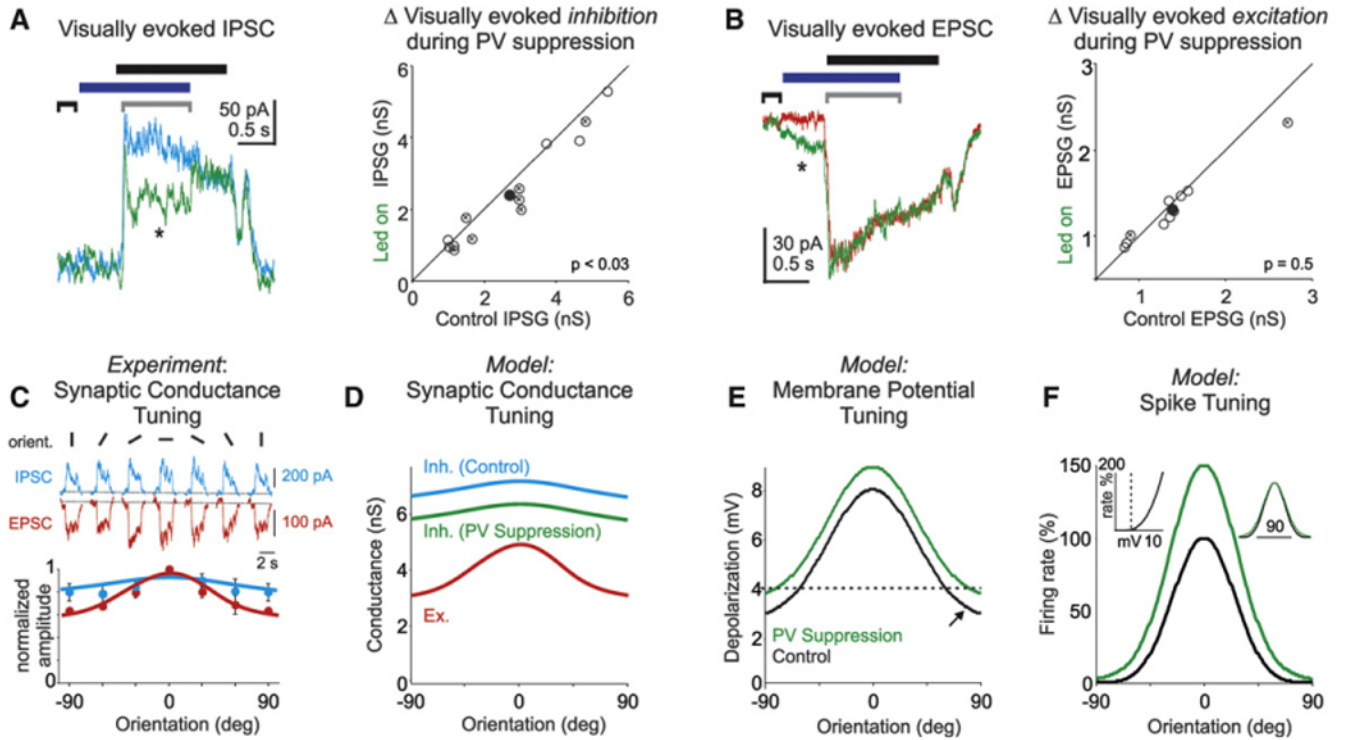
Figure 5. A Model Based on Experimentally Determined Synaptic Conductances Captures Linear Transformation of Pyr Cell Responses

(A) Left: visually evoked inhibitory postsynaptic currents (IPSC) recorded in a Pyr cell during control (cyan) and PV cell suppression (green). Average of 38 sweeps at each condition. Horizontal bars: black, stimulus presentation; blue, LED illumination. Brackets: black, baseline; gray, time over which average IPSC amplitude is computed. Right: scatter plot of visually evoked inhibitory conductance in control versus during PV cell photo suppression (open circles); "X" marks individual cells with significant change in conductance. Solid circle illustrates mean. Average decrease ~10%; n = 13; p < 0.03.

(B) Left: visually evoked excitatory postsynaptic currents (EPSC) recorded in a Pyr cell during control (red) and PV cell photo suppression (green). Average of 62 sweeps at each condition; horizontal bars and brackets as above. Note that while there is no change in the visually evoked EPSCs relative to baseline (black bracket), a significant increase in EPSC amplitude occurred systematically at led onset (asterisk; 0.1 ± 0.02 nS; n = 10; p < 0.004). Right: scatter plot of visually evoked excitatory conductance in control versus during PV cell photo suppression (open circles); "X" marks individual cells with significant change in conductance; solid circle illustrates mean. Excitatory conductance did not change significantly; n = 10; p = 0.5).

(C) Top: visually evoked IPSCs (cyan) and EPSCs (red) recorded in a layer 2/3 Pyr cell during the presentation of six sinusoidal grating orientations. Bottom, dots: summary of excitatory (red; n = 4) and inhibitory (cyan; n = 5) tuning as a function of orientation. Error bars are the SEM. Lines are the respective Gaussian fits.

(D) Tuning of excitatory synaptic conductance (red) and inhibitory synaptic conductance (cyan: control; green: during PV cell suppression, i.e., 10% reduction) as a function of orientation. Lines are the Gaussian fits from (C).

(E) Net depolarization in the membrane potential of modeled cell (resulting from conductances in D) as a function of orientation under control conditions (black) and during

PV cell suppression (green). The dotted line illustrates the spike threshold. Note that under control conditions the membrane potential is above threshold at most orientations.

(F) Model cell's orientation tuning, i.e., firing rate as a function of orientation under control conditions (black; OSI = 0.67; HWHH = 24 degrees) and during PV cell suppression (green; OSI = 0.59; HWHH = 26 degrees). Inset, left: the expansive nonlinear threshold or power law, i.e., the firing rate as a function of net membrane potential depolarization. Inset, right: orientation tuning curves in normalized to the peak. A 10% decrease in inhibition, as experimentally determined, results in ~50% increase in spiking response at the preferred orientation, a modest decrease in OSI (ΔOSI = 0.08), and a negligible change in tuning sharpness (ΔHWHH = 2 degrees).

Table 1

Conductance-Based Model Parameters

	Parameters
Leak Conductance	$g_L = 6$ nS; $R_L = -50$ mV
Excitatory Synaptic Conductance	$\sigma = 45$ deg; $g_{max} = 5$ nS; $g_{min} = 3$ nS; $R_E = 0$ mV (see Figure 5)
Inhibitory Synaptic Conductance	$\sigma = 70$ deg; $g_{max} = 7$ nS; g_{min} 6 nS; $R_I = -65$ mV (see Figure 5)